Research Article

INTERNATIONAL JOURNAL OF ADVANCED ROBOTIC SYSTEMS

International Journal of Advanced Robotic Systems
July-August 2017: 1–17

DOI: 10.1177/1729881417716592
journals.sagepub.com/home/arx
SAGE

A novel human-carrying quadruped walking robot

Lingfeng Sang[1,2], Hongbo Wang[2], Hongnian Yu[3] and Luige Vladareanu[4]

Abstract

This article adopts a 2-UPS+UP (U, P, and S are universal joint, the prismatic joint, and sphere joint, respectively) parallel mechanism as the leg mechanism of the quadruped walking robot based on the bionic concept and the motion capacity of the leg mechanism. The article investigates the kinematics (including the leg mechanism and the whole mechanism), gait planning, control, and experiment in detail. The following tasks are conducted: (1) designing the whole mechanism and developing the kinematics equations for both the leg mechanism and the whole mechanism; (2) planning the trotting gait and designing the foot trajectory based on the robot characteristics and conducting the kinematics analysis; (3) building the control system of the robot using self-developed controllers and drivers and studying the compound position control strategy; and (4) conducting the experiments for validating the controller, the compound position control strategy, the trotting pace, carrying capacity, and human-carrying walking. The results confirm that the proposed human-carrying walking robot has good performance and it is also verified that the controller and the compound position control strategy are suitable.

Keywords

Human-carrying walking, parallel leg mechanism, carrying capacity, kinematics analysis, experiment research

Date received: 11 March 2016; accepted: 1 June 2017

Topic: Climbing and Walking Robots
Topic Editor: Manuel Armada

Introduction

Walking aids have been an attractive research topic for a number of years.[1] A human-carrying walking robot, which is a type of walking aids, can help elderly and the lower limb disabled people walk freely in the outside environment and on uneven ground.

The human-carrying walking robot is different from wheeled robots and ordinary legged robots. It not only needs to walk steadily using the leg mechanism as a supporting point[2,3] but also has to bear a total weight comprising both its own weight and the load.[4] These create higher requirements for the leg mechanism performance of the walking chair robot. At present, most of the human-carrying walking robots for elderly and the lower limb disabled people are implemented using the serial mechanism to be the walking chair's leg mechanism,[5–9] such as the i-foot robot, the Hubo FX-1 robot, and the Hyperion4 robot. Using the serial mechanism as a leg mechanism, the whole volume and weight of the robot are greater and the carrying capacity is smaller. For instance, the i-foot robot weights 200 kg and it can only carry a 60 kg person; Hubo FX-1

[1] College of Mechanical and Electrical Engineering, Ningbo Polytechnic, Ningbo, People's Republic of China
[2] Parallel Robot and Mechatronic System Laboratory of Hebei Province, Yanshan University, Qinhuangdao, People's Republic of China
[3] School of Design, Engineering and Computing, Bournemouth University, Bournemouth, UK
[4] Robotics and Mechatronics, Real time control systems, Institute of Solid Mechanics, Institute of Solid Mechanics, Romanian Academy of Bucharest, Bucharest, Romania

Corresponding author:
Lingfeng Sang, No. 1069, New road, Beilun District, Ningbo, 315800, People's Republic of China.
Email: sanglingfeng@163.com

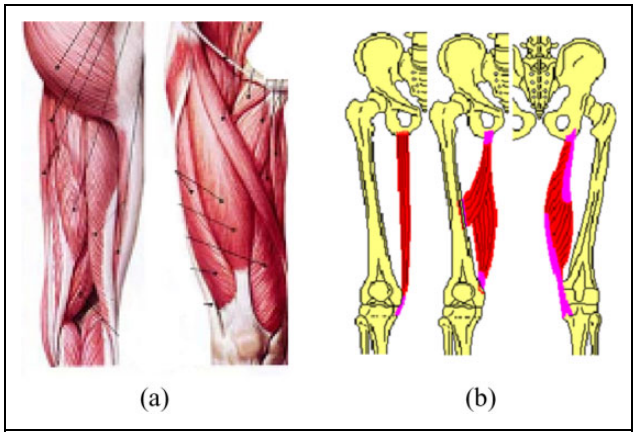

Figure 1. Human leg system. (a) Anatomic assembly. (b) Link diagram of muscle and skeletal.

weights 150 kg and it can only sustain a 100 kg load. Compared with the serial mechanism, parallel mechanism (PM) can overcome the deficiencies of the serial mechanism and form a complementary relationship with the serial mechanism.[10–12] For example, the WL-16RIV biped walking chair robot designed by Waseda University, Japan, weights 68 kg and can carry up to an 80 kg person. On the other hand, observing the animal motion systems (including human), it is noted that skeletal muscles are attached to the bones by tendons and arranged in a parallel way (shown in Figure 1). This parallel-link way of animal is similar to the PM. So PM is one of the better choices for the leg mechanism of a human-carrying walking robot.

Since the PM with limited-DOF (degrees of freedom) has the advantages being a simple mechanical structure with low cost for design, manufacturing, and control, the PM with less than 6-DOF is widely used. Analyzing the leg mechanism of the human-carrying walking robot, we conclude that it needs 3-DOF (swing back and forth, swing left and right, and lifting up and down). Considering manufacturing costs, the universal joint and the linear actuator could be purchased and each branch of PM includes these two kinematic pairs as soon as possible. Therefore, the mechanism configurations for meeting the motion and low-cost requirement are symmetrical 3-UPU PM,[13] 3-PUU PM,[14] 3-RPS PM,[15] and asymmetrical 2-UPS+UP PM, UPS+SPR+SP PM and UPS+UP+UPR PM. The 3-UPU PM is difficult to ensure that the axis of the two universal joints for each branch is parallel when the installation is finished.[16] As a leg mechanism, the arrangement of the prismatic joint for 3-PUU PM is difficult to achieve. If the 3-RPS PM is selected for the leg mechanism of the walking chair robot, then the walking chair robot may not move because of constraint forces coupling between branches. For asymmetrical UPS+SPR+SP PM and UPS+UP+UPR PM, it is difficult to realize a modular design and to low-cost manufacturing.

The manufacture cost of 2-UPS+UP PM is lower. For its UPS branch, there is no constraint on the moving platform, the motion of the whole asymmetrical PM is determined by the UP branch.[17] So we select 2-UPS+UP PM as the leg mechanism of the human-carrying walking robot.

Gait planning of the walking robot depends on the leg structure and the number of legs, for example, the eight-legged imitation crab robot,[18] the gecko-like robot,[19,20] the hexapod robot,[21] and the biped robot.[22–24] For the same robot, the planned gait depends on the various states of motion such as free walking gait,[25] climbing stair gait,[26] turning gait,[27] and trotting gait[28] for the quadruped robot.

Compared with the general quadruped robot, the leg structure of the human-carrying walking robot studied in this article is different. To the best of the authors' knowledge, there is little work available for its gait planning.

Generally, the gait of a quadruped robot can be divided into static walking gait and dynamic walking gait. Employing the static walking gait for a robot, the inertial forces are ignored. Using the dynamic walking gait, the inertial forces are considered. The static walking gait includes the crawl gait and the amble gait. The dynamic walking gait mainly includes the gallop gait, the trot gait, the bouncing gait, and the unilateral jogging gait.

Passenger safety is the most important requirement of the human-carrying walking robot. So the walking speed of the robot has to be limited to provide a comfortable transport for the passenger. Comparing the static and the dynamic walking gait and considering the structure of the walking robot, the trotting gait with a modification is selected as the motion gait of the walking robot.

The article is organized as follows. "Design of the whole mechanism" section describes design of the whole mechanism and establishes the coordinate system. In the section "Kinematics analysis of the walking robot," kinematics for the parallel leg mechanism (PLM) and the whole mechanism are analyzed in detail. In the section "The foot trajectory and trotting gait planning," based on kinematics, the trotting gait is planned and the foot trajectory is designed. In the section "Experiment research of the walking robot," experiment researches for the leg mechanism and the whole walking robot are conducted.

Design of the whole mechanism

The prototype of the human-carrying walking robot is shown in Figure 2. The whole mechanism consists of a seat, a connection plate, four PLMs, and a control system. Among them, the seat, the connection plate, and the control system are collectively called the body mechanism.

The PLM consists of the upper platform, the lower platform, two UPS branches, and one UP branch. Joint S of the UPS branch is made up of one rotation joint and one universal joint (as shown in Figure 3(a)). According to the performance analysis of the walking robot[17] and the market

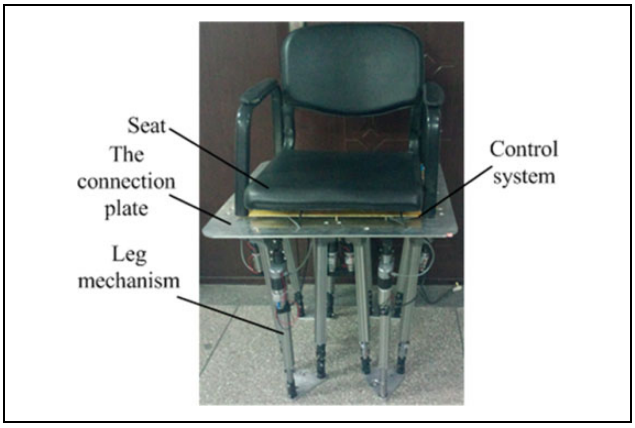

Figure 2. Human-carrying walking robot.

information, the structural design parameters of the walking chair robot are defined as follows. The rotational range for each axis of the universal joint is $-\pi/2$ to $\pi/2$. Joint P is realized by the linear actuator and the range is from 441 mm to 741 mm. Both of the upper and lower platforms are equilateral triangles, and a and b are their sides, respectively. ϕ and φ are angles of the triangles for the upper platform and the lower platform, respectively. t_1 and t_2 are the thickness of the upper platform and the lower platform, respectively. d_1 is the distance between the connecting hole of connector 1 and the end face of the upper platform. d_2 is the distance between the center of universal joint and the connecting hole of universal joint. d_3 is the distance between the two connecting holes of connector 2. d_4 is the distance between the two connecting holes of connector 3.

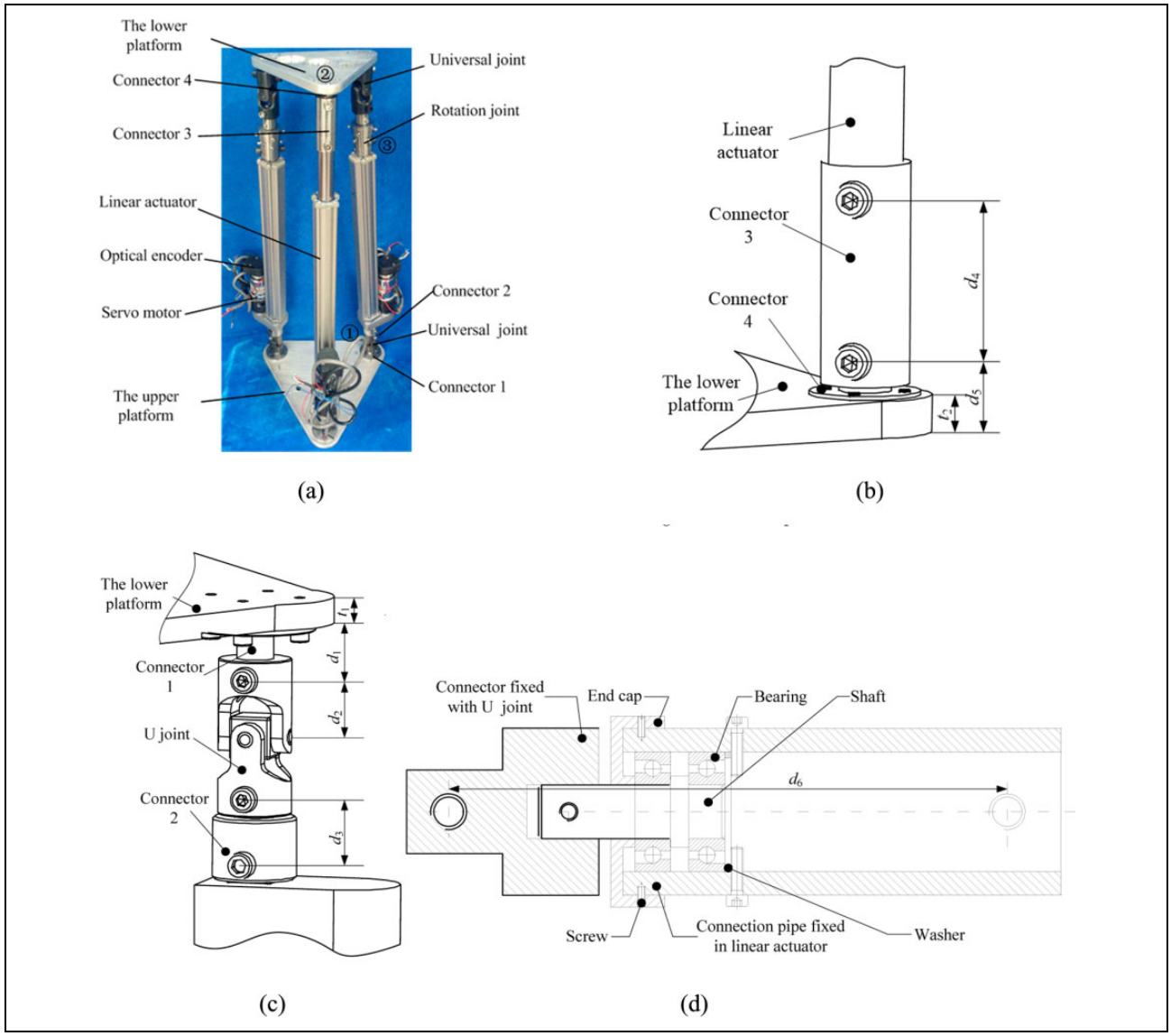

Figure 3. (a) 2-UPS+UP PM. (b) A larger version of position 2 in (a). (c) A larger version of position 3 in (a). (d) Internal structure of the rotation joint.

Table 1. Design parameters for the leg mechanism of the walking chair robot.

Parameter	Value	Parameter	Minimum	Value	Maximum
A	200 mm	P joint	441 mm	—	741 mm
B	120 mm	U joint	$-\pi/2$	—	$\pi/2$
d_1	21 mm	d_6		62 mm	
d_3	25 mm	d_2	—	23 mm	—
d_4	44 mm	d_5	—	20 mm	—
t_1	10 mm	t_2		10 mm	
ϕ	$\pi/3$	Φ		$\pi/3$	

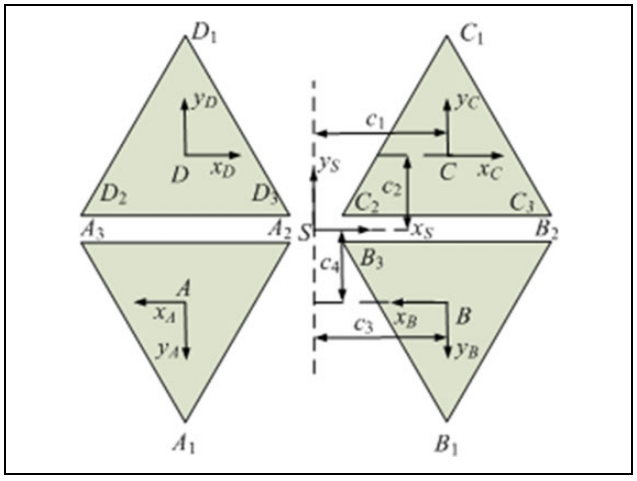

Figure 4. Arrangement of the upper platform of the leg mechanism on the connection plate.

d_5 is the distance between the connecting hole of connector 4 and the end face of the lower platform. d_6 is the length of the rotation joint. The design values of these parameters are shown in Table 1 and the structure is shown in Figure 3(b) to (d).

The upper platform of the PLM is fixed on the connection plate. The arrangement for the upper platform of the PLM which is fixed on the connection plate is shown in Figure 4. In the figure, c_1, c_2, c_3, and c_4 are arrangement parameters and their values are $c_1 = c_3 = 155$ mm and $c_2 = c_4 = 142.3$ mm. In each PLM, starting from the UP branch, the hinge point of the upper platform with each branch is numbered in the counterclockwise direction. The coordinate frames for the center of the PLM are established. Taking leg 1 as an example, A_1, A_2, and A_3 are the hinge points of one UP branch, two UPS branches, respectively. The coordinate frame $\{A\}$: A-$x_Ay_Az_A$ is established at point A. x_A is parallel to A_2A_3. y_A is vertical to A_2A_3. z_A is determined by the right-hand screw rule. The body coordinate frame $\{S\}$: S-$x_sy_sz_s$ is established at the center of the body mechanism. y_s is parallel to y_c and it is the movement direction for the front and the back of the body mechanism. x_s is parallel to x_c and it is the movement direction for the left and the right of the body mechanism. z_s is determined by the right-hand screw rule.

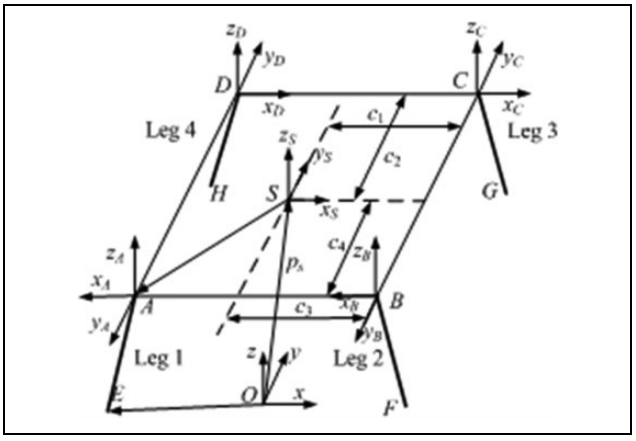

Figure 5. The coordinate system of the whole mechanism.

From Figure 4, the coordinate frame of the whole mechanism is established as shown in Figure 5. The global coordinate frame $\{O\}$: O-xyz is established on the ground. Under the initial position, each axis direction of the global frame is the same with the body mechanism. The points E, F, G, and H are the centers of the lower platform of legs 1, 2, 3, and 4, respectively.

Kinematics analysis of the walking robot

In this section, kinematics analysis for the PLM is studied firstly and then the kinematics equations for the body mechanism are derived.

Kinematics analysis of the leg mechanism

The upper platform A is installed on the connection plate. When the PLM is swinging, it can be considered that the upper platform A is fixed and the lower platform E is moving along X_E and Y_E relative to the upper platform A.

Inverse position analysis for the leg mechanism. In the inverse position analysis, it is assumed that the reference point position on the lower platform E is known, in order to find the length change of each branch.

If E_1 is selected to be the reference point, then the computing process of each branch length change is described below.

According to the coordinate frame established in Figure 6, each point of the upper platform in the coordinate frame $\{A_1\}$ can be described as

$$\boldsymbol{A}_1 = \begin{bmatrix} 0 \\ 0 \\ 0 \end{bmatrix}, \ \boldsymbol{A}_2 = \begin{bmatrix} -as(\phi/2) \\ -ac(\phi/2) \\ 0 \end{bmatrix}, \ \boldsymbol{A}_3 = \begin{bmatrix} as(\phi/2) \\ -ac(\phi/2) \\ 0 \end{bmatrix} \tag{1}$$

where $s(\phi/2) = \sin(\phi/2)$ and $c(\phi/2) = \cos(\phi/2)$.

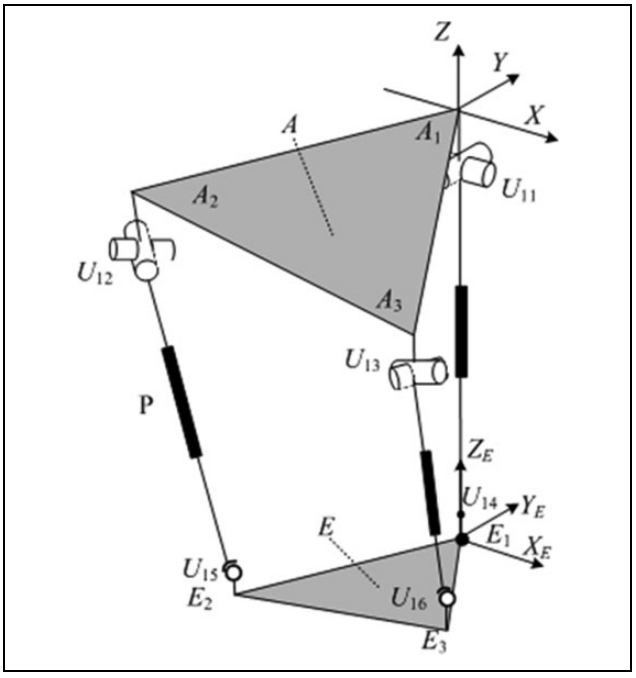

Figure 6. 2-UPS+UP PM schematic diagram.

The center point of the upper universal joint in the coordinate frame $\{A_1\}$ can be written as

$$\boldsymbol{U}_{11}=\begin{bmatrix}0\\0\\-x_1\end{bmatrix},\ \boldsymbol{U}_{12}=\begin{bmatrix}-as(\phi/2)\\-ac(\phi/2)\\-x_1\end{bmatrix},\ \boldsymbol{U}_{13}=\begin{bmatrix}as(\phi/2)\\-ac(\phi/2)\\-x_1\end{bmatrix} \tag{2}$$

where x_1 is the design size of the leg mechanism and $x_1=t_1+d_1+d_2$.

Each point of the lower platform in the coordinate frame $\{E_1\}$ can be described as

$$\boldsymbol{E}'_1=\begin{bmatrix}0\\0\\0\end{bmatrix},\ \boldsymbol{E}'_2=\begin{bmatrix}-bs(\varphi/2)\\-bc(\varphi/2)\\0\end{bmatrix},\ \boldsymbol{E}'_3=\begin{bmatrix}bs(\varphi/2)\\-bc(\varphi/2)\\0\end{bmatrix} \tag{3}$$

The lower end point of the UP branch and the center point of the lower universal joint in the UPS branch can be expressed as

$$\boldsymbol{U}'_{14}=\begin{bmatrix}0\\0\\x_2\end{bmatrix},\ \boldsymbol{U}'_{15}=\begin{bmatrix}-bs(\varphi/2)\\-bc(\varphi/2)\\x_3\end{bmatrix},\ \boldsymbol{U}'_{16}=\begin{bmatrix}bs(\varphi/2)\\-bc(\varphi/2)\\x_3\end{bmatrix} \tag{4}$$

where x_2 and x_3 are the design sizes of the leg mechanism and $x_2=d_5$ and $x_3=d_2+d_5$.

Each point in the coordinate frame $\{E_1\}$ could be transformed to the coordinate frame $\{A_1\}$ as

$$\boldsymbol{U}_{1k}={}^{A}\boldsymbol{R}_{E_1}\boldsymbol{U}'_{1k}+\boldsymbol{E}_1\ \ (k=4,5,6) \tag{5}$$

where $i=1,2,3$, ${}^{A}\boldsymbol{R}_{E_1}$ is the rotation transformation matrix from the moving coordinate frame to the global coordinate frame and

$${}^{A}\boldsymbol{R}_{E_1}=\begin{bmatrix}x_l & y_l & z_l\\ x_m & y_m & z_m\\ x_n & y_n & z_n\end{bmatrix}$$

$\boldsymbol{E}_1$ is the position vector of point E_1 and $\boldsymbol{E}_1=[E_{1x}\quad E_{1y}\quad E_{1z}]^{\mathrm{T}}$.

Because of the UP branch constraint, the PLM has the geometric constraints relationship as

$$\boldsymbol{R}_1\perp\boldsymbol{R}_2,\boldsymbol{R}_2\perp\boldsymbol{n}_{11},\boldsymbol{n}_{11}//\boldsymbol{Z}_E,\boldsymbol{R}_2//\boldsymbol{X}_E \tag{6}$$

where $\boldsymbol{R}_1$ and $\boldsymbol{R}_2$ are the first and second revolute axes of the universal joint U of branch UP, respectively and $\boldsymbol{n}_{11}$ is the direction vector of the UP branch.

According to the established coordinate frame, we obtain

$$\boldsymbol{R}_1=\begin{bmatrix}0\\1\\0\end{bmatrix},\quad \boldsymbol{R}_2=\begin{bmatrix}x_l\\x_m\\x_n\end{bmatrix},\quad \boldsymbol{n}_{11}=\frac{1}{l_{11}}(\boldsymbol{U}_{14}-\boldsymbol{U}_{11}) \tag{7}$$

where l_{1i} is the length change of each branch.

Substituting equations (4), (5), and (7) into equation (6) gives

$$\begin{cases}x_m=0\\ E_{1x}=-(l_{11}+x_2)z_l\\ E_{1y}=-(l_{11}+x_2)z_m\\ E_{1z}=-(l_{11}+x_2)z_n-x_1\end{cases} \tag{8}$$

According to equation (8), *Y–X–Z* Euler angles are selected, and we obtain the final transformation matrix as

$${}^{A}\boldsymbol{R}_{E_1}=\begin{bmatrix}c\alpha & s\alpha s\beta & s\alpha c\beta\\ 0 & c\beta & -s\beta\\ -s\alpha & c\alpha s\beta & c\alpha c\beta\end{bmatrix} \tag{9}$$

where α and β represent the rotation angles along the *Y*- and *X*-axes in the global coordinate frame.

Combining equation (8) with equation (9) leads to the following expressions

$$\begin{aligned} l_{11}&=\sqrt{(E_{1x})^2+(E_{1y})^2+(E_{1z}+x_1)^2}-x_2\\ \alpha&=\arctan\left(\frac{E_{1x}}{x_1+Z_E}\right)\\ \beta&=\arcsin\left(\frac{E_{1y}}{l_{11}+x_2}\right)\end{aligned} \tag{10}$$

The length change of each branch could be expressed as

$$\boldsymbol{l}_{1i}=\boldsymbol{U}_{1k}-\boldsymbol{U}_{1i}{}^{1i1i}\ \ (i=1,2,3\ \text{ and }\ i\neq 1) \tag{11}$$

According to equation , expressions for the length change of UPS branch could be derived as

$$l_{12} = \sqrt{\begin{array}{l}(-bs(\varphi/2)c\alpha - bc(\varphi/2)s\alpha s\beta + x_3 s\alpha c\beta + E_{1x} + as(\varphi/2))^2 + (-bc(\varphi/2)c\beta \\ -x_3 s\beta + E_{1y} + ac(\varphi/2))^2 + (bs(\varphi/2)s\alpha - bc(\varphi/2)c\alpha s\beta + x_3 c\alpha c\beta + E_{1z} + x_1)^2\end{array}}$$
$$l_{13} = \sqrt{\begin{array}{l}(bs(\varphi/2)c\alpha - bc(\varphi/2)s\alpha s\beta + x_3 s\alpha c\beta + E_{1x} - as(\varphi/2))^2 + (-bc(\varphi/2)c\beta - x_3 s\beta \\ +E_{1y} + ac(\varphi/2))^2 + (-bs(\varphi/2)s\alpha - bc(\varphi/2)c\alpha s\beta + x_3 c\alpha c\beta + E_{1z} + x_1)^2\end{array}} \quad (12)$$

If point E_2 is selected to be the reference point, the length change analysis process of each branch is described below.

Point E_2 relative to the coordinate frame $\{A_1\}$ can be described as

$$\boldsymbol{E}_2 = \begin{bmatrix} -bs(\varphi/2)c\alpha - bc(\varphi/2)s\alpha s\beta - (l_{11} + x_2)s\alpha c\beta \\ -bc(\varphi/2)c\beta + (l_{11} + x_2)s\beta \\ bs(\varphi/2)s\alpha - bc(\varphi/2)c\alpha s\beta - (l_{11} + x_2)c\alpha c\beta - x_1 \end{bmatrix} \quad (13)$$

where $\boldsymbol{E}_2 = [E_{2x} \quad E_{2y} \quad E_{2z}]^{\mathrm{T}}$.

From equation (13), we have

$$l_{11} + x_2 = \sqrt{E_{2x}^2 + E_{2y}^2 + (E_{2z} + x_1)^2 - b^2} \quad (14)$$

Let $u = \tan(\alpha/2)$, $v = \tan(\beta/2)$, and $t_m = l_{11} + x_2$. The second term of equation (13) can be simplified as

$$\Big(bc(\varphi/2) - E_{2y}\Big)v^2 + 2t_m v - \Big(E_{2y} + bc(\varphi/2)\Big) = 0 \quad (15)$$

Solving equation (15) gives

$$v = \frac{-t_m \pm \sqrt{t_m^2 + \Big(bc(\varphi/2) - E_{2y}\Big)\Big(E_{2y} + bc(\varphi/2)\Big)}}{\Big(bc(\varphi/2) - E_{2y}\Big)} \quad (16)$$

Similarly, simplifying the first component of equation (13) gives

$$\Big(bs(\varphi/2) - E_{2x}\Big)u^2 - 2\Big(bc(\varphi/2)s\beta + t_m c\beta\Big)u - \Big(bs(\varphi/2) + E_{2x}\Big) = 0 \quad (17)$$

Solving equation (17) gives

$$u = \frac{\Big(bc(\varphi/2)s\beta + t_m c\beta\Big) \pm \sqrt{\Big(bc(\varphi/2)s\beta + t_m c\beta\Big)^2 + \Big(bs(\varphi/2)\Big)^2 - E_{2x}^2}}{\Big(bs(\varphi/2) - E_{2x}\Big)} \quad (18)$$

According to the range of the angles α and β, we have that $v > 0$ and $u > 0$. Thus, the angles α and β can be considered as

$$\begin{aligned} \alpha &= \arctan(2u) \\ \beta &= \arctan(2v) \end{aligned} \quad (19)$$

Combining equations (11), (12), and (19), the length change of each branch can be obtained.

If point E_3 is selected as the reference point, then the analysis process is similar to point E_2.

Velocity analysis and acceleration for the leg mechanism. According to equation (11), the length change of each branch in the PLM can be rewritten as

$$\begin{aligned} \boldsymbol{l}_{11} &= l_{11}\boldsymbol{n}_{11} \\ \boldsymbol{l}_{11} + \boldsymbol{b}_{12} &= \boldsymbol{a}_{12} + \boldsymbol{l}_{12} \\ \boldsymbol{l}_{11} + \boldsymbol{b}_{13} &= \boldsymbol{a}_{13} + \boldsymbol{l}_{13} \end{aligned} \quad (20)$$

where $\boldsymbol{l}_{1i}$ is the direction vector of each branch, $\boldsymbol{b}_{12} = \boldsymbol{U}_{15} - \boldsymbol{U}_{14}$, $\boldsymbol{a}_{12} = \boldsymbol{U}_{12} - \boldsymbol{U}_{11}$, $\boldsymbol{b}_{13} = \boldsymbol{U}_{16} - \boldsymbol{U}_{14}$, and $\boldsymbol{a}_{13} = \boldsymbol{U}_{13} - \boldsymbol{U}_{11}$.

Taking derivative on both sides of each equation in (20), we have the velocity of each branch

$$\begin{aligned} \boldsymbol{v}'_{11} &= \dot{l}_{11}\boldsymbol{n}_{11} + \boldsymbol{w}_{11} \times l_{11}\boldsymbol{n}_{11} \\ \boldsymbol{v}'_{11} &= \dot{l}_{12}\boldsymbol{n}_{12} + \boldsymbol{w}_{12} \times l_{12}\boldsymbol{n}_{12} - \boldsymbol{w}_{11} \times \boldsymbol{b}_{12} \\ \boldsymbol{v}'_{11} &= \dot{l}_{13}\boldsymbol{n}_{13} + \boldsymbol{w}_{13} \times l_{13}\boldsymbol{n}_{13} - \boldsymbol{w}_{11} \times \boldsymbol{b}_{13} \end{aligned} \quad (21)$$

where $\boldsymbol{n}_{1i}$ is the direction vector of each branch, $\dot{l}_{1i}$ is the velocity along the direction of each branch, and $\boldsymbol{w}_{1i}$ is the angular velocity of each branch.

Taking the dot product $\boldsymbol{n}_{1i}$ on both sides of each equation in (21), we have the following equation

$$\dot{\boldsymbol{q}}_1 = \begin{bmatrix} \boldsymbol{n}_{11}{}^{\mathrm{T}} & 0 \\ \boldsymbol{n}_{12}{}^{\mathrm{T}} & (\boldsymbol{b}_{12} \times \boldsymbol{n}_{12})^{\mathrm{T}} \\ \boldsymbol{n}_{13}{}^{\mathrm{T}} & (\boldsymbol{b}_{13} \times \boldsymbol{n}_{13})^{\mathrm{T}} \end{bmatrix} \begin{bmatrix} \boldsymbol{v}'_{11} \\ \boldsymbol{w}_{11} \end{bmatrix} \quad (22)$$

where $\dot{\boldsymbol{q}}_1 = [\dot{l}_{11} \quad \dot{l}_{12} \quad \dot{l}_{13}]^{\mathrm{T}}$.

Meanwhile, the velocity of the reference point $\boldsymbol{E}_i$ can be expressed as

$$\boldsymbol{v}_{1i} = \boldsymbol{v}'_{11} + \boldsymbol{w}_{11} \times \boldsymbol{b}_{1k} \tag{23}$$

where $\boldsymbol{b}_{14} = \boldsymbol{E}_{11} - \boldsymbol{U}_{14}$, $\boldsymbol{b}_{15} = \boldsymbol{E}_{12} - \boldsymbol{U}_{14}$, and $\boldsymbol{b}_{16} = \boldsymbol{E}_{13} - \boldsymbol{U}_{14}$.

Taking the cross product $\boldsymbol{n}_{11}$ on both sides of the first equation in (21), we get the relationship between the angular velocity $\boldsymbol{w}_{11}$ and the velocity of point U_{14} of the UP branch as

$$\boldsymbol{w}_{11} = \frac{\boldsymbol{n}_{11} \times \boldsymbol{v}'_{11}}{l_{11}} \tag{24}$$

Combining equations (22) and (24) gives

$$\dot{\boldsymbol{q}}_1 = \boldsymbol{J}_{1m}\boldsymbol{v}'_{11} \tag{25}$$

where

$$\boldsymbol{J}_{1m} = \begin{bmatrix} \boldsymbol{n}_{11}{}^{\mathrm{T}} \\ \left(\boldsymbol{n}_{12} + \dfrac{(\boldsymbol{b}_{12} \times \boldsymbol{n}_{12}) \times \boldsymbol{n}_{11}}{l_{11}}\right)^{\mathrm{T}} \\ \left(\boldsymbol{n}_{13} + \dfrac{(\boldsymbol{b}_{13} \times \boldsymbol{n}_{13}) \times \boldsymbol{n}_{11}}{l_{11}}\right)^{\mathrm{T}} \end{bmatrix}$$

using the same procedure, equation (23) is transformed as

$$\boldsymbol{v}_{1i} = \boldsymbol{J}'_{1i}\boldsymbol{v}'_{11} \tag{26}$$

where

$$\boldsymbol{J}'_{1i} = I - \frac{S(\boldsymbol{b}_{1k})S(\boldsymbol{n}_{11})}{l_{11}}$$

and $\boldsymbol{S}(*)$ is the antisymmetric matrix.

If the inverse matrix of $\boldsymbol{J}'_{1i}$ exists, then the transitive relation between the input and output for velocity of the leg mechanism can be expressed as

$$\dot{\boldsymbol{q}}_1 = \boldsymbol{J}_{1i}\boldsymbol{v}_{1i} \tag{27}$$

where $\boldsymbol{J}_{1i} = \boldsymbol{J}_{1m}(\boldsymbol{J}'_{1i})^{-1}$.

Taking a derivative on both sides of equation (27), the transitive relation between the input and output for acceleration of the leg mechanism can be expressed as

$$\ddot{\boldsymbol{q}}_1 = \dot{\boldsymbol{J}}_{1i}\boldsymbol{v}_{1i} + \boldsymbol{J}_{1i}\boldsymbol{a}_{1i} \tag{28}$$

where $\ddot{\boldsymbol{q}}_1 = [\ddot{l}_{11} \quad \ddot{l}_{12} \quad \ddot{l}_{13}]^{\mathrm{T}}$, $\boldsymbol{a}_{1i}$ is the acceleration of the reference point E_i on the lower platform

$$\dot{\boldsymbol{J}}_{1i} = \dot{\boldsymbol{J}}_{1m}(\boldsymbol{J}'_{1i})^{-1} - \boldsymbol{J}_{1m}(\boldsymbol{J}'_{1i})^{-1}\dot{\boldsymbol{J}}'_{1i}(\boldsymbol{J}'_{1i})^{-1}$$

Kinematics analysis of the walking robot

Inverse position analysis of the walking robot. Inverse position analysis of the walking robot implies knowing the position ${}^{o}\boldsymbol{p}_s$ and posture ${}^{o}\boldsymbol{R}_s$ of the body mechanism, the reference point position of the lower platform of the standing leg, and the foot trajectory of the swing leg reference point, in order to solve the length change of each branch.

According to Figure 5, the position of closed-loop equation in each leg mechanism can be described as

$$\begin{aligned} {}^{o}\boldsymbol{p}_m &= {}^{o}\boldsymbol{p}_s + {}^{o}\boldsymbol{R}_s{}^{s}\boldsymbol{p}_m \\ {}^{s}\boldsymbol{p}_m &= {}^{s}\boldsymbol{p}_n + {}^{s}\boldsymbol{R}_n{}^{n}\boldsymbol{p}_m \end{aligned} \tag{29}$$

where $m = E, F, G, H$ and $n = A, B, C, D$. ${}^{o}\boldsymbol{p}_m$ is the position vector of point m in the global frame $\{O\}$. ${}^{o}\boldsymbol{R}_s$ is the rotation transformation matrix of the body coordinate frame $\{S\}$ relative to the global coordinate frame $\{O\}$. ${}^{s}\boldsymbol{p}_n$ is the position vector of the point n in the body coordinate frame $\{S\}$. ${}^{s}\boldsymbol{R}_n$ is the rotation transformation matrix of the coordinate frame $\{n\}$ relative to the body mechanism frame $\{S\}$. ${}^{n}\boldsymbol{p}_m$ is the position vector of the point m in the coordinate frame $\{n\}$.

The position vector for the reference point m_i of the lower platform in the leg mechanism relative to the leg mechanism coordinate frame $\{n\}$ is described as

$${}^{n}\boldsymbol{p}_{m_i} = {}^{n}\boldsymbol{p}_{n_1} + {}^{n}\boldsymbol{R}_{n_1}{}^{n_1}\boldsymbol{p}_{m_i} \tag{30}$$

where ${}^{n}\boldsymbol{p}_{n_1}$ is the position vector of point n_i in the coordinate frame $\{n\}$. ${}^{n}\boldsymbol{R}_{n_1}$ is the rotation transformation matrix of the coordinate frame $\{n_1\}$ relative to the coordinate frame $\{n\}$. ${}^{n1}\boldsymbol{p}_{m_i}$ is the position vector of the point m_i in the coordinate frame $\{n_1\}$.

Combining equations (29) and (30) gives

$${}^{n1}\boldsymbol{p}_{m_i} = ({}^{n}\boldsymbol{R}_{n_1})^{-1}(({}^{s}\boldsymbol{R}_n)^{-1}(({}^{o}\boldsymbol{R}_s)^{-1}({}^{o}\boldsymbol{p}_{m_i} - {}^{o}\boldsymbol{p}_s) - {}^{s}\boldsymbol{p}_n) - {}^{n}\boldsymbol{p}_{n_1}) \tag{31}$$

In equation (31), ${}^{n}\boldsymbol{R}_{n_1}$, ${}^{s}\boldsymbol{R}_n$, ${}^{s}\boldsymbol{p}_n$, and ${}^{n}\boldsymbol{p}_{n_{11}}$ are constant. ${}^{o}\boldsymbol{R}_s$, ${}^{o}\boldsymbol{p}_s$, and ${}^{o}\boldsymbol{p}_{m_{1i}}$ are known, therefore we can obtain ${}^{n1}\boldsymbol{p}_{m_i}$.

Combining inverse position analysis of the PLM and equation (31), the length change of each branch can be computed.

Velocity and acceleration analysis of the walking robot. Taking one derivative on both sides of each equation (29) and (30), we have

$$\begin{aligned} {}^{o}\dot{\boldsymbol{p}}_{m_i} &= {}^{o}\dot{\boldsymbol{p}}_s + S({}^{o}\boldsymbol{w}_s){}^{o}\boldsymbol{R}_s{}^{s}\boldsymbol{p}_{m_i} + {}^{o}\boldsymbol{R}_s{}^{s}\dot{\boldsymbol{p}}_{m_i}, \\ {}^{s}\dot{\boldsymbol{p}}_{m_i} &= {}^{s}\dot{\boldsymbol{p}}_n + S({}^{s}\boldsymbol{w}_n){}^{s}\boldsymbol{R}_n{}^{n}\boldsymbol{p}_{m_i} + {}^{s}\boldsymbol{R}_n{}^{n}\dot{\boldsymbol{p}}_{m_i}, \\ {}^{n}\dot{\boldsymbol{p}}_{m_i} &= {}^{n}\dot{\boldsymbol{p}}_{n_1} + S({}^{n}\boldsymbol{w}_{n_1}){}^{n}\boldsymbol{R}_{n_1}{}^{n_1}\boldsymbol{p}_{m_i} + {}^{n}\boldsymbol{R}_{n_1}{}^{n_1}\dot{\boldsymbol{p}}_{m_i}, \end{aligned} \tag{32}$$

where ${}^{o}\boldsymbol{w}_s$ is the angular velocity of the body mechanism center S relative to the global frame $\{O\}$. ${}^{o}\dot{\boldsymbol{p}}_s$ is the linear velocity of the body mechanism center S relative to the global frame $\{O\}$. ${}^{s}\dot{\boldsymbol{p}}_n = {}^{n}\dot{\boldsymbol{p}}_{n_1} = 0$ and ${}^{s}\boldsymbol{w}_n = {}^{n}\boldsymbol{w}_{n_1} = 0$.

Simplifying equation (32), the reference point velocity of the lower platform in the PLM can be obtained as

$${}^{n1}\dot{\boldsymbol{p}}_{m_i} = [-\boldsymbol{T}_1 \quad -\boldsymbol{T}_1{}^{o}\boldsymbol{R}_s\boldsymbol{S}({}^{s}\boldsymbol{p}_{m_i})] \begin{bmatrix} {}^{o}\dot{\boldsymbol{p}}_s \\ {}^{o}\boldsymbol{w}_s \end{bmatrix} + [\boldsymbol{T}_1 \quad 0] \begin{bmatrix} {}^{o}\dot{\boldsymbol{p}}_{m_i} \\ 0 \end{bmatrix} \tag{33}$$

where $\boldsymbol{T}_1 = ({}^{n}\boldsymbol{R}_{n_1})^{-1}({}^{s}\boldsymbol{R}_{n})^{-1}({}^{o}\boldsymbol{R}_{s})^{-1}$. There are two states in ${}^{o}\dot{\boldsymbol{p}}_{m_i}$. When the leg mechanism stands, ${}^{o}\dot{\boldsymbol{p}}_{m_i} = 0$; when the leg mechanism swings, ${}^{o}\dot{\boldsymbol{p}}_{m_i}$ is the planned foot trajectory.

Combining equations (27) and (33), the velocity of each branch could be obtained as

$$\dot{\boldsymbol{q}}_g = {}^{n_1}\boldsymbol{J}_{gi}{}^{n_1}\dot{\boldsymbol{p}}_{m_i} \tag{34}$$

where g is the serial number of the PLM and $g = 1, 2, 3, 4$.

Taking derivative on both sides of equation (33), acceleration ${}^{n1}\ddot{\boldsymbol{p}}_{m_i}$ of reference point m_i in the coordinate frame n_1 is derived as

$$\begin{aligned}{}^{n_1}\ddot{\boldsymbol{p}}_{m_i} = {} & \boldsymbol{T}_1{}^{o}\ddot{\boldsymbol{p}}_{m_i} - \boldsymbol{T}_1{}^{o}\ddot{\boldsymbol{p}}_{s} + \boldsymbol{S}({}^{o}\varepsilon_s)\boldsymbol{T}_2 + \boldsymbol{T}_1\boldsymbol{T}_3\boldsymbol{S}({}^{o}\boldsymbol{w}_s) \\ & + 2\boldsymbol{S}({}^{o}\boldsymbol{w}_s){}^{n_1}\dot{\boldsymbol{p}}_{m_i}\end{aligned} \tag{35}$$

where ${}^{o}\varepsilon_s$ is the angular acceleration for the center S of the body mechanism relative to the global frame $\{O\}$. ${}^{o}\ddot{\boldsymbol{p}}_s$ is the linear velocity for center S of the body mechanism relative to the global frame $\{O\}$. $\boldsymbol{T}_2 = \boldsymbol{T}_1{}^{o}\boldsymbol{R}_s\boldsymbol{S}({}^{s}\boldsymbol{p}_{m_i})$ and $\boldsymbol{T}_3 = \boldsymbol{S}({}^{o}\boldsymbol{w}_s){}^{o}\boldsymbol{R}_s\boldsymbol{S}({}^{s}\boldsymbol{p}_{m_i})$.

Combining equations (33)–(35), acceleration $\ddot{\boldsymbol{q}}_g$ for the walking robot is described as

$$\ddot{\boldsymbol{q}}_g = {}^{n_1}\boldsymbol{J}_{gi}{}^{n_1}\ddot{\boldsymbol{p}}_{m_i} + {}^{n_1}\dot{\boldsymbol{J}}_{gi}{}^{n_1}\dot{\boldsymbol{p}}_{m_i} \tag{36}$$

The foot trajectory and trotting gait planning

Motion planning of the robot is divided into two parts: the foot trajectory and the body motion.

The foot trajectory

The swing leg and the standing leg are the two motion states of the leg mechanism. The whole robot load is supported by the standing leg. The standing leg does not have relative motion between the foot and the ground. Thus the foot trajectory analysis is taken into account only for the swing leg.

A composite cycloid trajectory is proposed in the study by Sakakibara et al.[29] The cycloid trajectory is improved in the studies by Li et al.[28] and Wang et al.,[30] and two sections curve planning are applied for the swinging of the leg mechanism in the movement cycle. It results in drastic change of the synthetic acceleration and does not have the uniform speed motion process. Thus, three sections curve planning are used for the swinging of the PLM in this article.

Considering the first PLM motion in YA_1Z plane, no matter which axis the PLM swings relative to, the process of acceleration and deceleration is similar to the sine function and the expression is as follows

$$\ddot{y} = Am\sin\left(\frac{n\pi t}{T_m}\right) \tag{37}$$

where Am is the amplitude and T_m is the movement cycle of the swing leg.

Integrating the above formula, the following equation is derived

$$\dot{y} = -Am\frac{T_m}{2\pi}\cos\left(\frac{n\pi t}{T_m}\right) + C_1 \tag{38}$$

where C_1 is a constant.

According to the foot trajectory requirement, the curve should meet $\dot{y}|_{t=0} = 0$ and $\dot{y}|_{t=T_m} = 0$. The following equation is derived

$$C_1 = A\frac{T_m}{n\pi}, \quad n = 2k\ k = 1, 2, 3... \tag{39}$$

When $n = 2$, the trajectory is an oblique line in the YA_1Z plane. Although it is not conducive for the leg mechanism when crossing an obstacle, the trajectory referring to the Y-direction is suitable. As a result, the equation of displacement along Z is

$$y = S_0\left(\frac{t}{T_m} - \frac{1}{2\pi}\sin\left(2\pi\frac{t}{T_m}\right)\right) \tag{40}$$

When the n value is too large, it will result frequently in acceleration and deceleration moments along the Z-direction, which may not only cause the increasing of energy consumption but also induce the body mechanism tilting. In conclusion, $n = 4$ is selected for the Z-direction. The trajectory is divided into three sections along the Z-direction. $k_1T_m, k_2T_m,$ and k_3T_m are the motion time of the three sections and $k_1 + k_2 + k_3 = 1$. Supposing $k_1 = k_3 = 0.25$ and $k_2 = 0.5$, we have

$$\ddot{z} = \begin{cases} A\sin\left(\dfrac{4\pi t}{T_m}\right) & 0 \le t \le 0.25T_m \\ -B\sin\left(\dfrac{2\pi t}{T_m} - \dfrac{\pi}{2}\right) & 0.25T_m \le t \le 0.75T_m \\ C\sin\left(\dfrac{4\pi t}{T_m} - 3\pi\right) & 0.75T_m \le t \le T_m \end{cases} \tag{41}$$

where $A, B,$ and C are the amplitudes of the three sinusoids.

Integrating equation (41) twice, the following displacement curve is obtained

$$z=\begin{cases} -A\dfrac{T_m}{4\pi}\dfrac{T_m}{4\pi}\sin\left(\dfrac{4\pi t}{T_m}\right) & +C_1\ t+C_4 \qquad 0\le t\le 0.25T_m \\ B\dfrac{T_m}{2\pi}\dfrac{T_m}{2\pi}\sin\left(\dfrac{2\pi t}{T_m}-\dfrac{\pi}{2}\right) & +C_2\ t+C_5 \quad 0.25T_m\le t\le 0.75T_m \\ -C\dfrac{T_m}{4\pi}\dfrac{T_m}{4\pi}\sin\left(\dfrac{4\pi t}{T_m}-3\pi\right) & +C_3\ t+C_6 \quad 0.75T_m\le t\le T_m \end{cases} \tag{42}$$

According to the requirement of the foot trajectory, the curve should meet $\dot{z}|_{t=0}=0$, $\dot{z}|_{t=T_m/2}=0$, $\dot{z}|_{t=T_m}=0$, $z|_{t=0}=0$, $z|_{t=T_m/2}=H$, and $z|_{t=T_m}=0$. Meanwhile, each section is successive. Finally, the coefficient expressions of equation (42) can be obtained

$$\begin{gathered} A=B=C=\frac{16\pi^2 H}{{T_m}^2(4+\pi)},\quad C_1=-C_3=\frac{4\pi H}{(4+\pi)T_m},\quad C_2=C_4=0 \\ C_5=\frac{\pi H}{4+\pi},\quad C_6=\frac{4\pi H}{4+\pi} \end{gathered} \tag{43}$$

Substituting equation (43) into equation (42), the displacement cycloid equation can be obtained along the *Z*-direction as

$$z=\begin{cases} \dfrac{H}{(4+\pi)}\left(\dfrac{4\pi}{T_m}t-\sin\left(\dfrac{4\pi t}{T_m}\right)\right) & 0\le t\le 0.25T_m \\ \dfrac{4H}{(4+\pi)}\left(\sin\left(\dfrac{2\pi t}{T_m}-\dfrac{\pi}{2}\right)+\dfrac{\pi}{4}\right) & 0.25T_m\le t\le 0.75T_m \\ \dfrac{4\pi H}{(4+\pi)}\left(1-\dfrac{t}{T_m}-\dfrac{1}{4\pi}\sin\left(\dfrac{4\pi t}{T_m}-3\pi\right)\right) & 0.75T_m\le t\le T_m \end{cases} \tag{44}$$

Trotting gait planning

To the trotting gait, the human-carrying walking robot in this article is different from a general quadruped robot. The foot of the general quadruped robot is sphere, and when the foot is in contact with the ground, the point is formed. Thus, when performing the trotting gait, a straight line is made by leg mechanisms as the supporting area. Under this condition, stability of the robot is poor. Our proposed human-carrying quadruped walking robot with PLM performs differently since the surface contact is formed when its feet are in contact with the ground. Thus, the supporting polygon area still exists. There are two gait forms: 13-24 and 24-13 gait. The following analysis uses the 13-24 trotting gait as an example. Figure 7 shows the planning diagram of the 13-24 trotting gait. Center of Gravity (COG) indicates the gravity center position of the human-carrying walking robot. The closed polygon formed by red lines is the support polygon area of the walking robot. The motion process of the human-carrying walking chair is as follows:

1. Step 1: Leg 1 and leg 3 make a step first, respectively, as shown in Figure 7(a).
2. Step 2: When step 1 finishes, the body mechanism is adjusted, as shown in Figure 7(b).
3. Step 3: Leg 2 and leg 4 make a step, respectively, after the adjustment of the body mechanism ends, as shown in Figure 7(c).

This cyclical gait only needs three steps.

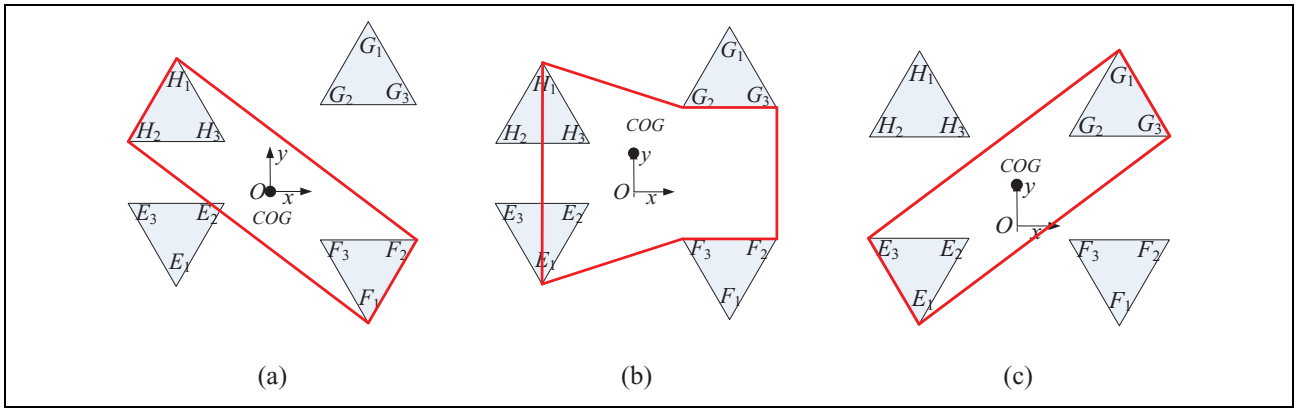

Figure 7. Trotting gait 13-24 with individual adjustment the center of gravity. (a) Swing leg 1 and leg 3. (b) Adjusting the body mechanism. (c) Swing leg 2 and leg 4.

Trotting gait simulation

In order to verify the theory analysis correctness of trotting gait planning and the foot trajectory, the trotting gait simulation is conducted. Assuming the initial state of the walking chair robot is when the UP branch is perpendicular to the ground, the initial height is $H_0 = 665.4$ mm, the highest amplitude of the foot trajectory is $H = 100$ mm, the step size is $S_0 = 102.7$ mm, and the period of motion is $T_m = 5$ s. The body mechanism motion function is

$$\begin{cases} x_s = 0, \quad y_s = 0, \quad z_s = 22.94t & 0 \le t \le 5 \\ x_s = 0, \quad y_s = 0, \quad z_s = 114.7 & 5 < t \le 10 \\ x_s = 0, \quad y_s = 20.54(t-10), \quad z_s = 114.7 & 10 < t \le 15 \\ x_s = 0, \quad y_s = 102.7, \quad z_s = 114.7 & 15 < t \le 20 \\ x_s = 0, \quad y_s = 102.7, \quad z_s = 114.7 - 22.94(t-20) & 20 < t \le 25 \end{cases} \tag{45}$$

The swing leg mechanism is conducted using equations (40) and (44). Based on these motion functions and the mechanism parameters, the simulation is realized, as shown in Figure 8.

Based on the simulation results, we can draw the following conclusions:

1. Leg mechanism 1 and leg mechanism 4 show a symmetric changing rule; leg mechanism 2 and leg mechanism 3 also show the symmetric changing rule. The simulation results highlight the symmetry and consistency, which shows that the kinematics model of the human-carrying walking chair robot is valid.
2. In the periods of 0–5 s, 10–15 s, and 20–25 s, the change for each branch of the leg mechanism is caused by the motion of the body mechanism. In the periods of 5–10 s and 15–20 s, the change of each branch is caused by the foot trajectory. Therefore, we find that the velocity change of each branch is discontinuous (in Figure 8(b)), but the motion of the walking robot is continuous.
3. The acceleration changes of the leg mechanism are smooth and there is no impact with ground in case of the origin position and terminal position, which shows that the foot trajectory planning is suitable.
4. According to the design of the PLM, it can be seen that the length range of the UP branch is in the interval of 591.4–891.4 mm and the velocity range is between 0 and 80 mm/s; the length range of the UPS branch is between 574 and 874 mm and the velocity range is between 0 and 80 mm/s. From Figure 8(a) and(b), it can be seen that their values are in the motion range.

Experiment research of the walking robot

Control system

For the robot, the controller and the driver are developed by our own research group, which are shown in Figure 9. One controller and one driver are used for each motor. The main control chip of the controller is PIC18F452 single chip computer, and the CPLD chip of the driver is XC9536-7VQ44C. This controller can realize three control modes (position control, velocity control, and current control), and the three control modes can be switched at any time.

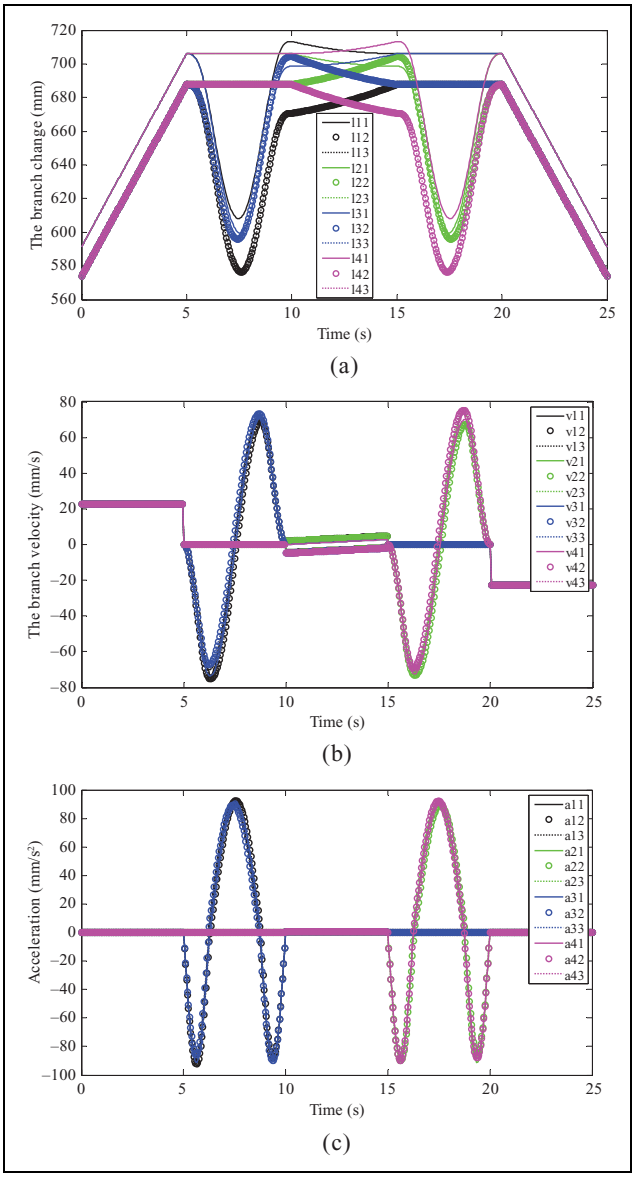

Figure 8. Trotting gait simulation. (a) The length change of all branches. (b) Velocity curves of all branches. (c) Acceleration curves of all branches.

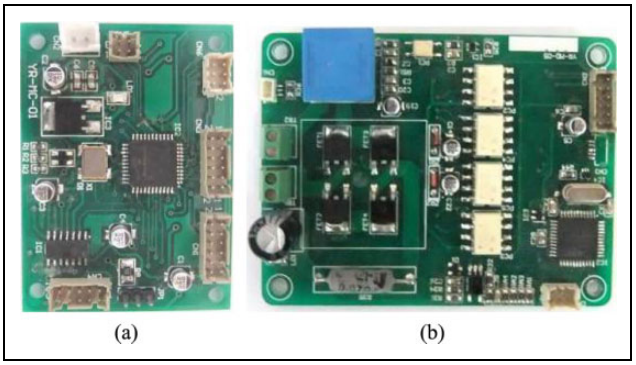

Figure 9. (a) The controller and (b) the driver of motor.

If the position control mode is used, then the motor runs at its maximum velocity but its work velocity cannot be guaranteed; if the velocity control mode is adopted, then the motor runs at the specified velocity but its target position cannot be ensured. Based on these two control modes, the compound position control method is proposed. The method is that, firstly, the motor is controlled using the velocity mode between two discrete position nodes, meanwhile the position of the motor is detected and the accumulation error of the position is computed in this control period. And the desired velocity in the next control period is modified by applying the error. Finally, the target position and the work velocity can be guaranteed. The schematic diagram of the whole process is shown in Figure 10.

According to Figure 10, the accumulation error of the position in this control period is

$$\Delta p_e = p_d - p_r \tag{46}$$

where p_d is the theoretical position and p_r is the measured position.

The work velocity for the next control period is

$$v'_d = P\Delta p_e + v_d \tag{47}$$

where P is a proportional constant.

The velocity Proportional-Integral (PI) control law is

$$Pr\_v = k_p(v'_d - v_r) + k_i\sum(v'_d - v_r) \tag{48}$$

where k_p and k_i are proportional constant and integration constant, respectively, and v_r is the measured velocity.

Experiment research of PLM 1

To verify the feasibility of the controller and the compound position control method, in this section, experiment research of PLM 1 is conducted based on the laser tracker Leica AT901. The process of the whole experiment is shown below:

1. In the optimal workspace of the leg mechanism,[31] the reference point E_1 of the lower platform is planned as

$$\begin{cases} E_{1x} = 100\cos\left(\dfrac{2\pi}{5}t - \dfrac{\pi}{2}\right) \\ E_{1y} = 100 + 100\sin\left(\dfrac{2\pi}{5}t - \dfrac{\pi}{2}\right) \\ E_{1z} = -675.4 \end{cases} \tag{49}$$

2. Based on equation (48) and inverse kinematics of the PLM, the position and the velocity of the three branches are computed using a simulation software, as shown in Figure 11.

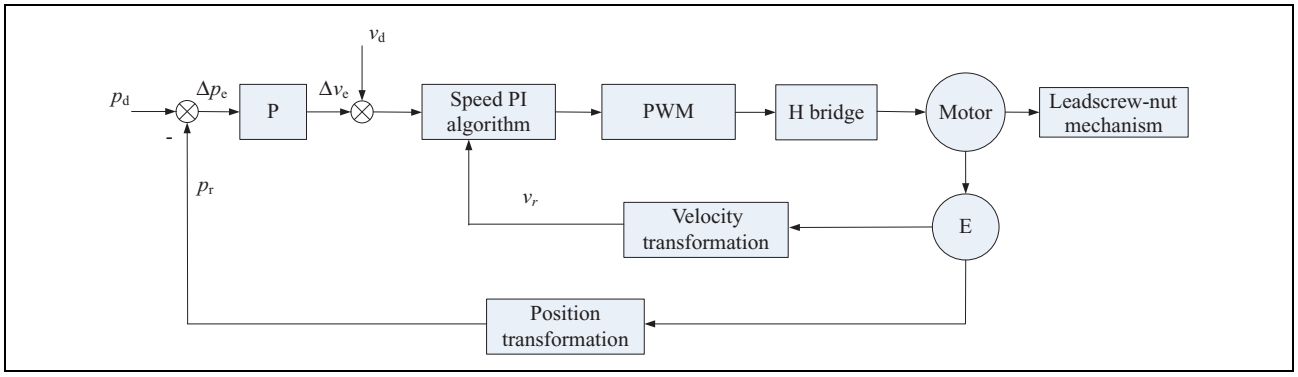

Figure 10. Compound position control method.

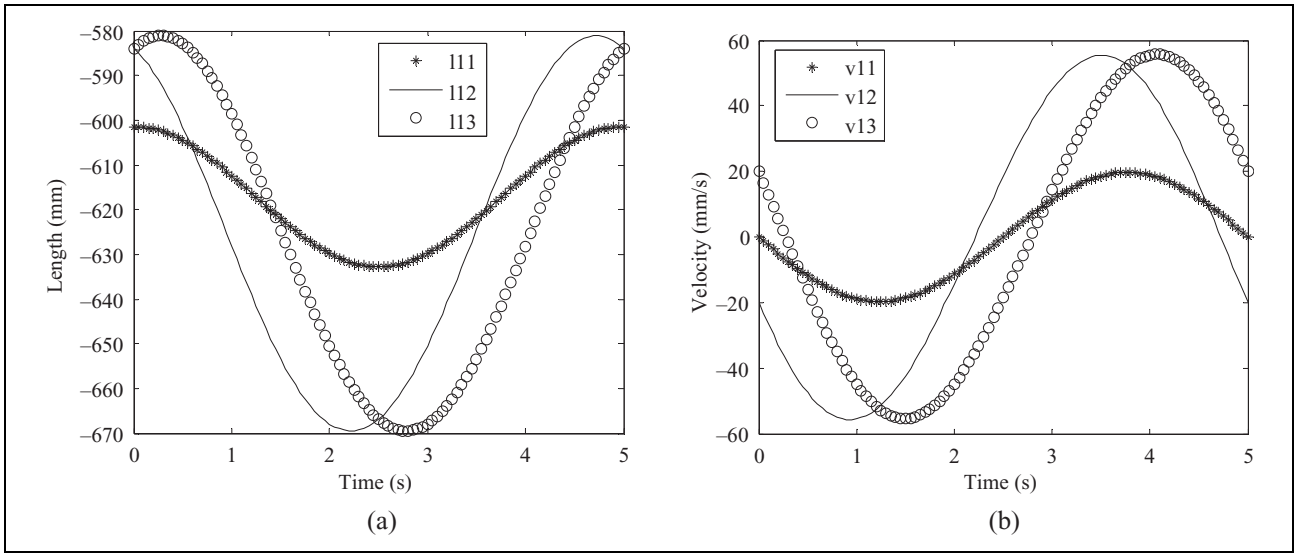

Figure 11. Inverse kinematics analysis of the leg mechanism. (a) The length change of three branches. (b) Velocity of three branches.

3. The position and velocity relative to 0 of three branches are obtained by offsetting the simulation data, and then the results are saved as a binary file to be loaded into the control program.
4. The control system and the measure system of the PLM are established as shown in Figure 12. The control system consists of three controllers, three drivers, Can bus, the power modular, and the host computer. The measure system includes the refection ball and the laser tracker.
5. Positions of four screw holes connected with the UP branch on the upper platform are measured using the Leica T-Probe handheld measuring sensor and then four records are saved. Based on these four records, the coordinate frame $\{A_1\}$ is established; meanwhile the initial position of the lower platform reference point E_1 is measured, as shown in Figure 13.
6. The magnetic device is mounted at the reference point E_1 on the lower platform of leg mechanism. The reflection ball is fixed on the magnetic device and it reflects the laser.
7. The leg mechanism works in accordance with the planning trajectory and then the experimental data are saved in an excel file.

Finally, the theoretical curve and the experiment curve are shown in Figure 14, where we can draw the following conclusions:

1. The experiment trajectory is closely related to the theoretical trajectory. However, there are some errors at the initial position and the end position due to the mechanism error. Comparing the radius of theoretical trajectory with the radius of experiment trajectory, the maximum error is 2.454 mm.
2. The experiment trajectory of the leg mechanism is stable and the fluctuation is little noticeable. Thus, the designed controller is suitable for the experiment requirement.
3. The position error of the whole motion process is not accumulated using the compound control

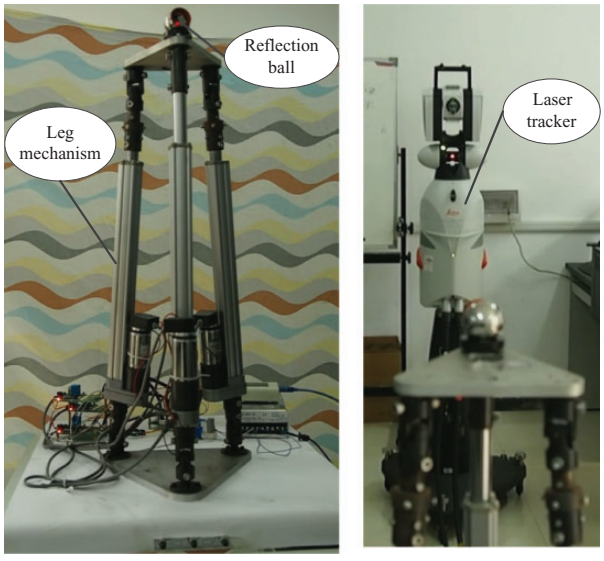

Figure 12. Trajectory tracking experiment of the leg mechanism. (a) Rear view. (b) Front view.

Figure 13. Establishing the coordinate system and measuring the initial position.

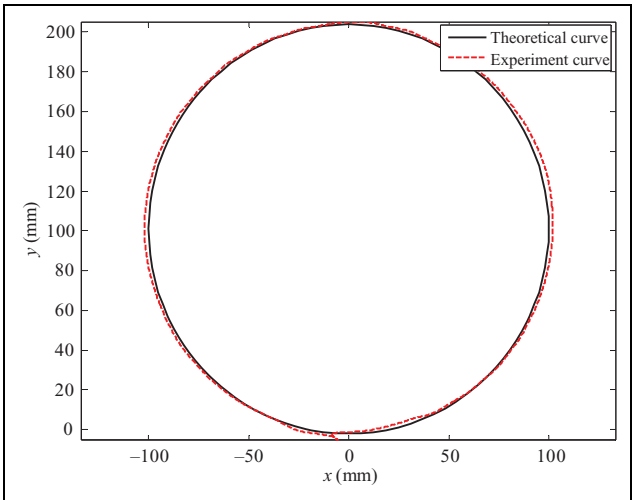

Figure 14. Contrast of theoretical value and experimental value.

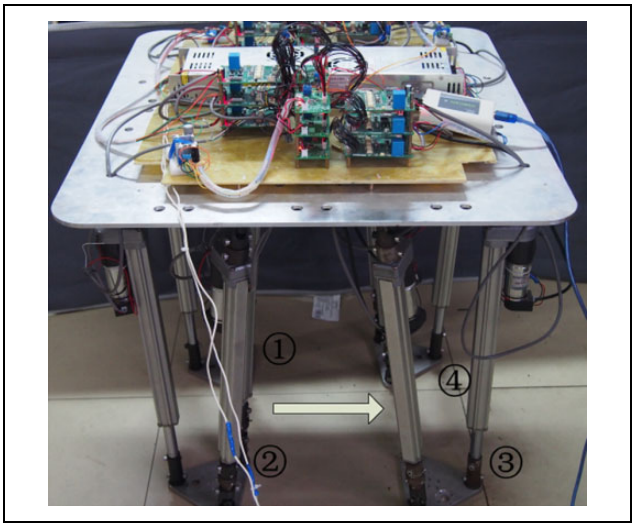

Figure 15. Number of the leg mechanism and motion direction of the robot.

method. Thus, the compound position control method is feasible.

Experiment research for the trotting gait of the walking robot

Based on the above theoretical analysis and experiment test of PLM 1, in this section, the trotting gait of the human-carrying walking robot is conducted. The serial number of leg mechanism and the motion direction are shown in Figure 15. And the motion process of the trotting gait is as shown in Figure 16. In these figures, the motions of Figure 16(a) and (e) are used to adjust the height of the body mechanism. The motions of Figure 16(b)–(d) are applied at the implement step.

During the process of the whole experiment, the motion of the human-carrying walking robot is in line with the theoretical gait planning and the gait has a smooth motion. Thus, the correctness and rationality of the trotting gait planning is verified.

Walking experiment research of the human-carrying walking robot

For the walk experiment, it is necessary to determine the payload capacity of the robot. The payload capacity is relative to many factors, such as the structural parameters, the structural arrangements, the thrust of linear actuator, the inertial force, the inertial moment, and so on. They could be expressed as the following equations

$$\boldsymbol{F}_{bw} + \boldsymbol{F}_q + (\boldsymbol{J}_q^s)^{\mathrm{T}} \boldsymbol{F}_s = \boldsymbol{B} \tag{50}$$

where $\boldsymbol{F}_{bw}$ is the external force and the external moment, $\boldsymbol{F}_q$ is the determined input force, $\boldsymbol{F}_s$ is the redundant input force, $\boldsymbol{J}_q^s$ is the transformed matrix of $\boldsymbol{F}_s$ from the

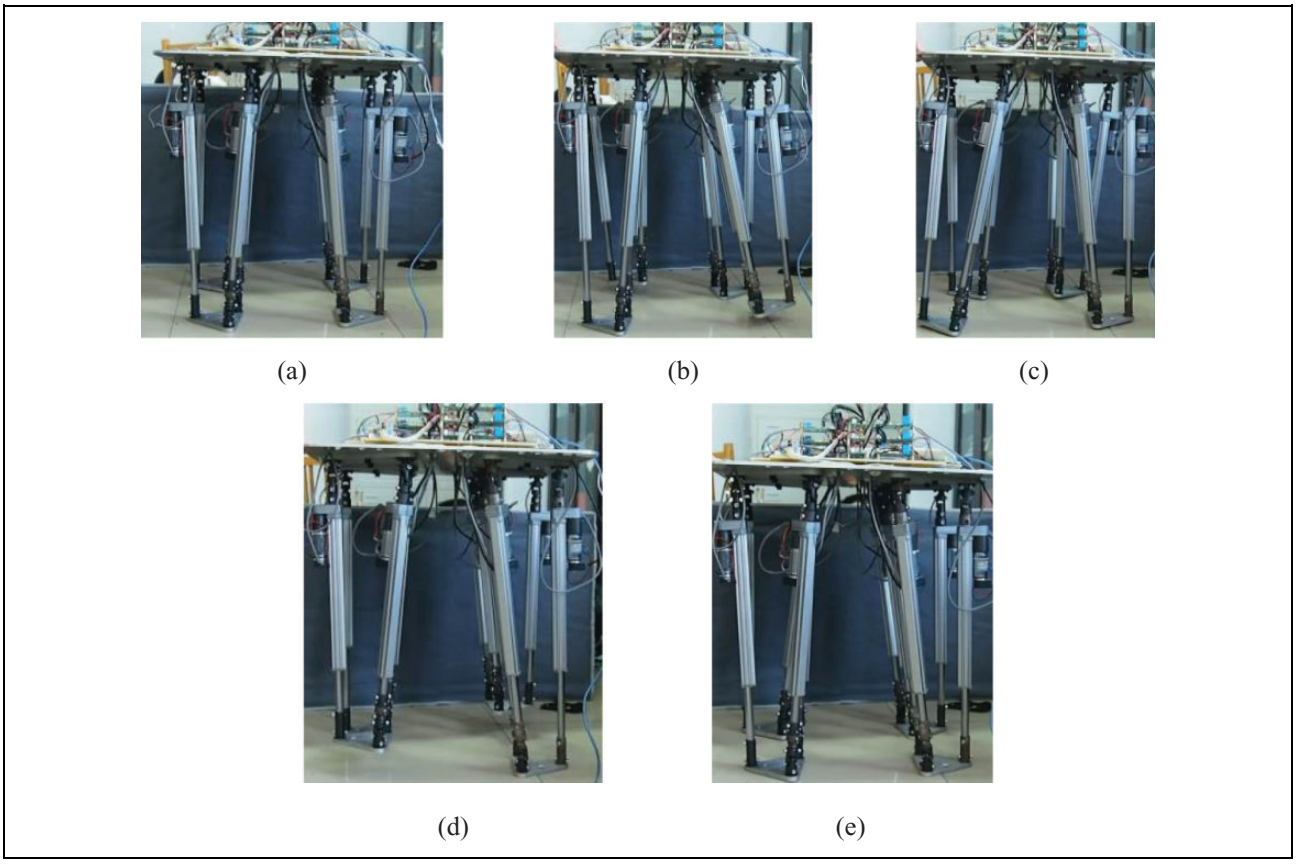

Figure 16. Motion of the dynamic walking gait 13-24. (a and c) Adjusting body mechanism. (b) Swing leg 1 and leg 3 mechanism. (d) Swing leg 2 and leg 4 mechanism. (e) Backing to the initial height.

non-generalized coordinate to the generalized coordinate, and $\boldsymbol{B}$ is described as

$$\boldsymbol{B} = -(\boldsymbol{F}_{b\_\text{inertial}} + \boldsymbol{F}_{fgi\_\text{inertial}} + \boldsymbol{F}_{xg\_\text{inertial}}) \tag{51}$$

where $\boldsymbol{F}_{b\_\text{inertial}}$ is the inertial force and the inertial moment of the body mechanism and the upper platform of the each leg mechanism, $\boldsymbol{F}_{fgi\_\text{inertial}}$ is the inertial force and the inertial moment of the each branch in the leg mechanism, $\boldsymbol{F}_{xg\_\text{inertial}}$ is the inertial force and the inertial moment of the lower platform in the leg mechanism.

When the structure and the motion trajectory of the robot are decided, the $\boldsymbol{B}$ is a constant. So we only need to check the strength of the key part. We analyze all the parts and find that the strength of the universal joint is the weakest. According to formula (52) of shear stress, the range of the shear stress can be decided

$$\tau = \frac{F}{A} \leq [\tau] \tag{52}$$

where $[\tau] = 98$ MPa and $A \approx 7.07$ mm^2. We can obtain $F \leq 692.86$ N.

According to the structural design of the robot, the thrust $\boldsymbol{F}_N$ of the linear actuator can be computed by the following equation

$$F_N = \frac{2\pi T_N \eta}{n_i P} \approx 427.3\,\text{N} \tag{53}$$

Comparing equations (52) and (53), we find that the structural strength of the universal joint is enough. So the thrust of the linear actuator can be described as

$$-F_N \leq f_{gi} \leq F_N \tag{54}$$

where f_{gi} is the thrust of each branch and $f_{gi} \in \boldsymbol{F}_q\ \boldsymbol{F}_s$.

Meanwhile, f_{gi} also can be described by the following equation

$$f_{gi} = C_t i \tag{55}$$

where C_t is a constant.

From equation (55), we observe that the current reflects the thrust of the linear actuator. We can obtain the payload weight by measuring the current of the each branch and the thrust is maximum when the current is maximum.

So we could add payload on the walking robot continuously and observe the current data of each branch. Figure 17 is the current change curve of each branch when the payload is 57 kg.

From these four figures, we can draw the following conclusions:

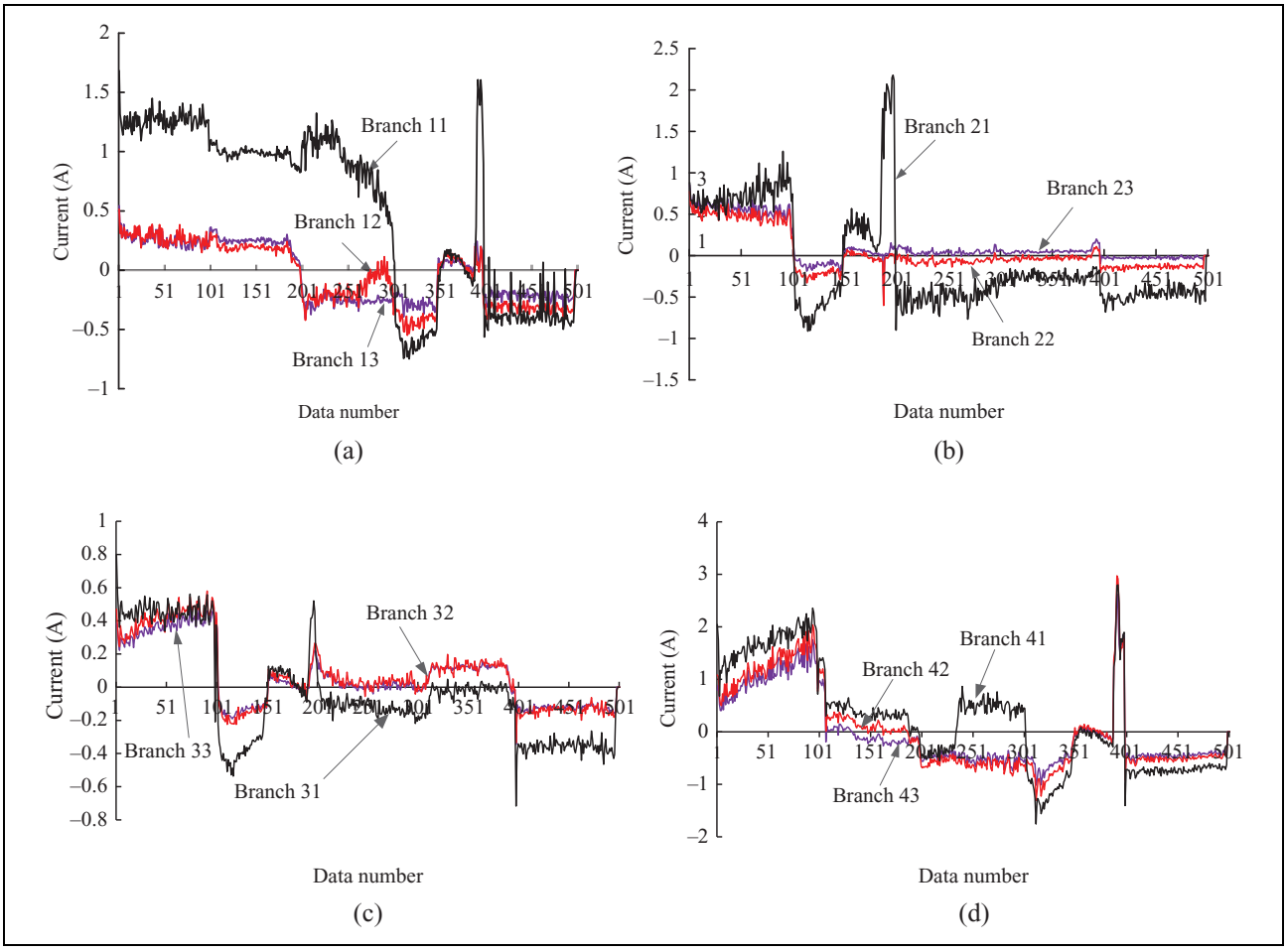

Figure 17. Current change curve for each leg mechanism of the human-carrying walking chair robot. Current change for each branch of (a) leg 1, (b) leg 2, (c) leg 3, and (d) leg 4.

1. The current change of the branches 2 and 3 of each leg mechanism is the same. The result is consistent with the motion law.
2. The current change for branch 1 of each PLM is the maximum, such as branch 11 with 1.7 A, branch 21 with 2.4 A, branch 31 with 0.6 A, and branch 41 with 3 A. We obtain that the rated current of the linear actuator is 3 A. So the maximum payload of the human-carrying walking robot is 57 kg.

Figure 18 shows the human-carrying experiment when the payload is 47.5 kg.

From the motion of human-carrying walking robot, we can obtain that the gait planning and the designed controller are reasonable, and the payload capacity is enough.

The walking chair robot is placed on an electronic platform scale, and the measured result is 49.2 kg, as shown in Figure 19. We find that the payload–weight ratio of the walking chair robot is 1.16. It is higher than i-foot robot, Hobo FX-1, and WL-16RIV. Thus, we conclude that the walking robot has great payload capacity.

Conclusions

1. Based on the 2-UPS+UP PM, the human-carrying quadruped walking chair robot with PLM has been proposed and the prototype has been designed and manufactured.
2. Combining the human-carrying walking chair robot, the kinematics for the leg mechanism and the body mechanism are derived. Through the experiment on simulating the foot trajectory and the trotting gait, we have verified that the kinematics model is valid.
3. The control system of the human-carrying quadruped walking robot has been designed, and the compound position control strategy has been studied. Through experiment verification, it is found that the controller and the driver are suitable to experiment requirements for the control system of walking chair robot and the compound position control strategy is feasible.
4. The trotting gait experiment of the human-carrying walking chair robot has been conducted and the results show that the motion of the human-

Figure 18. Human-carrying experiment of walking robot.

Figure 19. Weight measurement of the walking chair robot.

carrying walking chair robot is in line with the theoretical gait planning and the gait has a smooth motion. The correctness and rationality of the theory of planning gait has been verified.

5. Based on the current change of the linear actuator, we have concluded that the payload capacity of the human-carrying walking robot is 57 kg.

The present work will be extended in the future from the following two aspects:

1. *Mechanism optimization*: At present, the payload capacity of the walking chair robot is only 57 kg and is lower than the weight of an average person. So the whole walking chair robot will be optimized to increase the payload capacity of the walking chair robot in the future.
2. *Human in the loop control strategy research*: Because of changing with the height, weight, and motion of the passenger on the seat, the security and stability of the human-carrying walking chair robot are affected. We need to consider these changes when the control strategy is researched. In the future, we plan that the passenger is regarded as the loop of the control system and research on the passenger influence to the whole control system.

Declaration of conflicting interests

The author(s) declared no potential conflicts of interest with respect to the research, authorship, and/or publication of this article.

Funding

The author(s) disclosed receipt of the following financial support for the research, authorship, and/or publication of this article: This work is supported by National Natural Science Foundation of China (no. 61075099), Specialized Research Fund for the Doctoral Program of Higher Education (no. 20131333110006), FP7-PEOPLE-2012-IRSES: Marie Cuire Action "International Research Staff Exchange Scheme (no. 318902), and High-level Personnel Funded Project in Hebei Province.

References

1. Ping W, Dun XM, and Chen WD. The general overview of research on assistant robot. *Robot Techn Appl* 2009; 1: 31–34.
2. Liu J, Zhao XG, and Tan M. Legged robots: a review. *Robot* 2006; 28(1): 81–88.
3. Zhang JH, Zhang XJ, Zhang ML, et al. Eight wheel-legged mobile robot platform design and kinematic analysis. *Chin J Mach Des* 2012; 29(8): 35–39.
4. Zheng CY, Zhao QF, Ma PS, et al. Mechanism design of a biped walking-chair robot. *Robot* 2006; 28(3): 297–302.

5. Stefan K. On the anticipation of ethical conflicts between humans and robots in Japanese Mangas. *Int Rev Inf Ethics* 2006; 6(12): 63–68.
6. Kim JH, Kim JY, and Oh JH. Adaptive walking pattern generation and balance control of the passenger-carrying biped robot, HUBO FX-1, for variable passenger weights. *Auton Robots* 2011; 30: 427–443.
7. Nakajima S and Nakano E. Adaptive gait for large rough terrain of a leg-wheel robot (Fifth report: integrated gait). *J Robot Mechatron* 2009; 21(13): 419–426.
8. Yoneda K. Light weight quadruped with nine actuators. *J Robot Mechatron* 2007; 19(2): 160–165.
9. Tang J, Zhao Q, and Yang R. Stability control for a walking-chair robot with human in the loop. *Int J Adv Robotic Syst* 2009; 6(2): 115–120.
10. Sugahara Y, Carbone G, Hashimoto K, et al. Experimental stiffness measurement of WL-16RII biped walking vehicle during walking operation. *J Robot Mechatron* 2007; 19(3): 272–280.
11. Rong Y and Jin ZL. Dynamic modeling of 3-DOF parallel leg mechanism and peak prediction of servo motor. *Opt Precis Eng* 2012; 20(9): 1974–1982.
12. Wang HB, Qi ZY, Hu ZW, et al. Application of parallel leg mechanisms in quadruped/biped reconfigurable walking robot. *Chin J Mech Eng* 2009; 45(8): 24–30.
13. Tsai LW and Joshi S. Kinematics and optimization of a spatial 3-UPU parallel manipulator. *J Mech Des* 2000; 122: 439–446.
14. Guo ZH, Sun SS, Hao XQ, et al. Position analysis and simulation of 3-PUU translational parallel manipulator. *Chin Mech Eng* 2006; 17(17): 1787–1789.
15. Li QC, Chen Z, Chen QH, et al. Structural condition for [PP]S parallel mechanism without parasitic motion. *J Mech Eng* 2010; 46(15): 31–35.
16. Merlet JP. *Parallel robot*. 2nd ed. Dordrecht: Springer, 2006. pp. 31–35.
17. Sang LF, Wang HB, Zhang DF, et al. Application of parallel mechanism in varistructured quadruped/biped human-carrying walking chair robot. *Int J Autom Comput* 2013; 10(5): 447–454.
18. Wang G, Zhang L, and Wang QL. Research on a gait planning method for a crab-like octopod robot. *J Harbin Eng Univ* 2011; 32(4): 486–491.
19. Ruan P, Yu ZW, Zhang H, et al. Gait planning and simulation of gecko inspired robot based on ADAMS. *Robot* 2010; 32(4): 499–504.
20. Meng C, Wang TM, Guan SG, et al. Design and analysis of gecko-like robot. *Chin J Mech Eng* 2011; 24(4): 224–236.
21. Roy SS and Pratihar DK. Effects of turning gait parameters on energy consumption and stability of a six-legged walking robot. *Rob Auton Syst* 2012; 60(1): 72–82.
22. Kensuke H, Shuuji K, Fumio K, et al. Real-time planning of humanoid robot's gait for force-controlled manipulation. *IEEE/ASME Trans Mechatron* 2007; 12(1): 53–62.
23. Sugahara Y, Hashimoto K, Sunazuka H, et al. Towards the biped walking wheelchair. In: *IEEE/RAS-EMBS international conference on biomedical robotics and biomechatronics*, Pisa, 2006, p. 781–786.
24. Hashimoto K, Sugahara Y, Sunazuka H, et al. Biped landing pattern modification method with nonlinear compliance control. In: *IEEE international conference on robotics and automation*, Orlando, Florida, USA, 2006, pp. 1213–1218.
25. Wang BP, Hu RX, and Zhang XD. Gait planning and intelligent control for a quadruped robot. *J Control Theory Appl* 2009; 7(2): 207–211.
26. Huang B, Zhao JW, and Sun LN. Straight walking and stair climbing gait of quadruped robot based on static balance. *Robot* 2010; 32(2): 226–232.
27. Ma PS and Ma L. A study of turning gait control for quadruped walking vehicle. *J ShangHai Jiaotong Univ* 1995; 29(5): 87–92.
28. Li YB, Li B, Rong XW, et al. Mechanical design and gait planning of a hydraulically. *J ShanDong Univ (Eng Sci)* 2011; 41(5): 32–36.
29. Sakakibara Y, Kan K, Hosoda Y, et al. Foot trajectory for a quadruped walking machine. In: *IEEE international workshop on intelligent robots and systems*, Ibaraki, 1990, pp. 315–322.
30. Wang LP, Wang JZ, Wang SK, et al. Strategy of foot trajectory generation for hydraulic quadruped robots gait planning. *J Mech Eng* 2013; 49(1): 39–44.
31. Sang LF, Wang HB, Wang SS, et al. Theory analysis and experiment research of the leg mechanism for the human-carrying walking chair robot. *J Robot* 2014; 2014: 1–12.